Theor Chem Acc (2010) 127:641–650
DOI 10.1007/s00214-010-0763-1

REGULAR ARTICLE

Perfluorinated exohedral potassium-metallofullerene K···C_nF_n (n = 20 or 60): partial interior and surface excess electron state

Yin-Feng Wang · Ying Li · Zhi-Ru Li · Fang Ma · Di Wu · Chia-Chung Sun

Received: 11 February 2010 / Accepted: 3 May 2010 / Published online: 21 May 2010

Abstract The fullerene [60] can bind a variety of metal to form exohedral metallofullerenes with special chemical and physical properties. However, how about the structure and properties of the perfluorinated exohedral metallofullerene with excess electron? The structures of K···$C_{20}F_{20}$ (C_{5v}), K···$C_{60}F_{60}$ (C_{3v}), and K···$C_{60}F_{60}$ (C_{6v}) with all real frequencies are represented at the B3LYP/6-31G(d) theory level. The large ionization potentials of 7.066 ~ 7.422 eV suggest the large stabilities of them. Owing to the interpolarization between K and C_nF_n (n = 20 or 60) cage, an electron transfers from K atom to the perfluorinated cage ($C_{20}F_{20}$ or $C_{60}F_{60}$) to form excess electron and long $K^+\cdots C_nF_n^-$ ionic bond (length > 2.9 Å) with interaction energies of −78.24 ~ −93.72 kcal/mol. Comparing to the solvated electron $e^-@C_nF_n$ (n = 20 or 60) with interior state, under the effect of counterion K^+, partial excess electron is pulled from the interior to the surface of the cage to form partial interior and surface excess electron state. It is found that cage size and shape influence excess electron absorption spectrum, which may be important for the design of the new optical and photoelectric materials or devices with good performances.

Keywords Excess electron · Perfluorinated exohedral metallofullerene · Partial interior and surface state

Y.-F. Wang · Y. Li · Z.-R. Li (✉) · F. Ma · D. Wu · C.-C. Sun
State Key Laboratory of Theoretical and Computational Chemistry, Institute of Theoretical Chemistry, Jilin University, Changchun 130023, China
e-mail: lzr@jlu.edu.cn

1 Introduction

Since the discovery [1] and macroscopic production [2] of C_{60}, doped fullerenes with unique structures and electronic properties [3–9] have become a subject of intense investigations because of their potential application in the optical, magnetic, electronic, catalytic, and biological areas of materials science [10–14]. Much attention has been devoted to endohedral fullerenes [4–7]. Kim et al. have investigated the nature of the interaction between paramagnetic atoms A (=^{4}N, ^{4}P, ^{3}O, and ^{3}S) and C_{60} in the endohedral fullerenes (A@C_{60}) [7]. The exohedral fullerenes, in particular, exohedral metallofullerenes, [8, 9] in which the dopant atoms are located outside the fullerene cages, have attracted a lot of attentions concerning the effects of metal coordination on the chemical and physical properties of C_{60} as well as with the direct analogy to carbon nanotubes decorated by metal nanoparticles [15–19].

For the perfluorinated fullerene, the $C_{20}F_{20}$ has been obtained experimentally and theoretically [20–22]. In 1991, Halloway et al. [23] first suggested the existence of $C_{60}F_{60}$. Scuseria et al. [24, 25] confirmed this prediction by theoretical calculations (the same and next year) and pointed out that the synthesis difficulty of $C_{60}F_{60}$ comes from the thermodynamic forces against it. [26, 27] Recently, Wu and his co-workers [28] have theoretically studied the structure and stability of a set of large neutral $C_{60}F_{60}$ cages. It is wondering, however, whether or not a metal atom can be doped outside the perfluorinated fullerene cage to form perfluorinated exohedral metallofullerene? This is an interesting question.

The investigation of the excess electron [29, 30] plays a prominent role in physics, chemistry, and biochemistry [31–34]. Stabilization and manipulation of bound electrons

are important in molecular clusters and nano devices [35] and could provide new approaches to preparing conductive materials with unusual optical [36, 37] or magnetic properties [38–41]. As an excess electron is trapped by a polar solvent, such as water or ammonia, [42] the question of whether the excess electron is on the surface or in the interior of the clusters has been the subject of much speculation [43–48]. In addition, Jordan and his co-worker have identified a new binding motif, where the excess electron permeates the hydrogen-bonding network. [48] For the perfluorinated fullerene cage, $C_{20}F_{20}$ or $C_{60}F_{60}$ has large interior electronic attractive potential [51, 52] to confine an excess electron. Recently, the interesting cage-like single molecular solvated single electron systems with interior excess electron state, e.g. $e^-@C_{20}F_{20}$ and $e^-@C_{60}F_{60}$, are found [49–52]. As a dopant metal atom is located outside a perfluorinated fullerene cage, how about the behavior of the single electron of the metal atom? Does this electron still inhabit in the frontier orbital of the metal atom or be distributed to the perfluorinated fullerene cage? If this electron is distributed to the cage to form excess electron, it is wondering how about the effect of the counterion metal cation on the location of the excess electron? Is the excess electron encapsulated inside the perfluorinated cage or somewhere else? Considering the interpolarization between K and C_nF_n ($n = 20$ or 60) cage, how about cage size and shape effects on the structure and properties? These are worth investigating.

To answer these questions, in this paper, our investigation aims at obtaining the structures and stabilities of the perfluorinated exohedral potassium-metallofullerenes, $K\cdots C_{20}F_{20}$ (C_{5v}), $K\cdots C_{60}F_{60}$ (C_{3v}), and $K\cdots C_{60}F_{60}$ (C_{6v}), showing that an electron transfers from K atom to the perfluorinated cage ($C_{20}F_{20}$ or $C_{60}F_{60}$) to form excess electron and $K^+\cdots C_nF_n^-$ ($n = 20$ or 60) ionic bond, exhibiting the excess electron with the partial interior and surface state, revealing the evolution of the excess electron location, displaying the effect of the cage size and shape on the structures, stabilities, and electric properties, and enhancing the knowledge on excess electron chemistry and exohedral chemistry.

2 Computational details

For the geometry optimization, the structures of the neutral $C_{60}F_{60}$ cage [28] and $C_{20}F_{20}$ cage [51] have been successfully obtained by Wu and his co-workers at B3LYP/6-31G(d) density functional theory (DFT) level. In this work, for three perfluorinated exohedral potassium-metallofullerenes, $K\cdots C_{20}F_{20}$ (C_{5v}), $K\cdots C_{60}F_{60}$ (C_{3v}), and $K\cdots C_{60}F_{60}$ (C_{6v}), the calculations of geometrical optimizations, analytical vibrational frequencies, and the natural bond orbital (NBO) analysis [54, 55] were performed at B3LYP/6-31G(d) level.

There are many literatures about the controversy whether or not the density functional theory (DFT) can yield reasonably good electron affinities (EAs) [56, 57] or vertical electron detachment energies (VDEs) [58]. Schaefer's paper [56] pointed out that the B3LYP, BLYP, BP86, B3PW91, and BPW91 functionals are excellent choices for EA predictions and suggested that the basis set dependence of DFT functional is small. Recently, the VDEs of two $e^-@C_{60}F_{60}$ (I_h and D_{6h}) have been obtained with B3LYP method and the calculations also suggested the small basis set dependence [52]. The ionization potential (IP) value of 7.619 eV for C_{60} (I_h) at B3LYP/6-311 + G(2d)//B3LYP/6-31G(d) level is very close to the measured values of 7.565 eV [59, 60] for the stable C_{60}. Therefore, basing on the optimized neutral geometries, the IP and EA values of the $K\cdots C_nF_n$ ($n = 20$ or 60) were calculated at the B3LYP/6-311 + G(2d) level, which is performable with the available computer resources, as the following formulas:

$$\mathrm{IP} = E[\mathrm{K}\cdots\mathrm{C}_n\mathrm{F}_n^+] - E[\mathrm{K}\cdots\mathrm{C}_n\mathrm{F}_n]_{\mathrm{opt}} \quad (1)$$

$$\mathrm{EA} = E[\mathrm{K}\cdots\mathrm{C}_n\mathrm{F}_n]_{\mathrm{opt}} - E[\mathrm{K}\cdots\mathrm{C}_n\mathrm{F}_n^-] \quad (2)$$

The deformation energy E_{def} of the C_nF_n ($n = 20$ or 60) cage is defined as the energy difference between C_nF_n cage in the optimized $K\cdots C_nF_n$ and that in the optimized neutral C_nF_n structure. It was also calculated at the B3LYP/6-311 + G(2d) level as the following formulas:

$$E_{\mathrm{def}} = E[\mathrm{C}_n\mathrm{F}_n]_{\mathrm{optK}\cdots\mathrm{C}_n\mathrm{F}_n} - E[\mathrm{C}_n\mathrm{F}_n]_{\mathrm{opt}} \quad (3)$$

Truhlar et al. have suggested that a new hybrid meta exchange–correlation functional, called M05-2X, is one of the best functionals for the study of interaction energies and noncovalent interactions [61, 62]. Therefore, the interaction energies (E_{int}) were calculated at M05-2X/6-311 + G(2d) and B3LYP/6-311 + G(2d) level. To correct the basis-set superposition error (BSSE), [63] the counterpoise (CP) procedure [64, 65] was used in the calculations of interaction energies. The E_{int} is the difference between the energy of the exohedral compound and the sum of the energies of the metal K atom and the C_nF_n ($n = 20$ or 60) cage, as illustrated by the following formula: [63]

$$E_{\mathrm{int}} = E_{\mathrm{AB}}(X_{\mathrm{AB}}) - E_{\mathrm{A}}(X_{\mathrm{AB}}) - E_{\mathrm{B}}(X_{\mathrm{AB}}) \quad (4)$$

The same basis set, X_{AB}, was used for both the moieties and the exohedral compound.

The polarizability was computed at the HF/6-31 + G(d) level. The CIS/6-31G(d) calculations were performed to obtain the excess electronic absorption spectra.

The spin contamination is negligible, as the expected value of spin eigenvalue $<S^2>$ for each of these species is

0.75 in the calculations. All the calculations were performed with the GAUSSIAN 03 program package [66].

3 Results and discussions

3.1 Geometrical characteristics

The optimized geometric structures of the K···$C_{20}F_{20}$ (C_{5v}), K···$C_{60}F_{60}$ (C_{3v}), and K···$C_{60}F_{60}$ (C_{6v}) with all real frequencies at B3LYP/6-31G(d) level are depicted in Fig. 1. For the K···$C_{20}F_{20}$ (C_{5v}), the dopant K atom is outside a pentagonal carbon ring of the $C_{20}F_{20}$ cage, while the dopant K atom is outside a hexagonal carbon ring of the $C_{60}F_{60}$ cage for the K···$C_{60}F_{60}$ (C_{3v} and C_{6v}). The distances (h) between K atoms and the corresponding pentagonal or hexagonal carbon rings are 2.943 ~ 3.045 Å. The lengths of K···F in these structures are 2.770 ~ 2.901 Å, which are evidently larger than that of the isolated K–F molecule (2.174 Å at B3LYP/6-31G(d) level and 2.177 Å at CCSD(T)/6-31G(d) level). Recently, the neutral perfluorinated fullerenes, $C_{20}F_{20}$ (I_h) [51] and $C_{60}F_{60}$ (I_h and D_{6h}) [28], and the single molecular solvated electron systems, $e^-@C_{20}F_{20}$ (I_h) [51] and $e^-@C_{60}F_{60}$ (I_h and D_{6h}) [52], have been reported. Comparing the K···C_nF_n ($n = 20$ or 60) with the corresponding C_nF_n or $e^-@C_nF_n$ (see Table 1), it can be found that the doping effect obviously decreases the symmetry of the molecule.

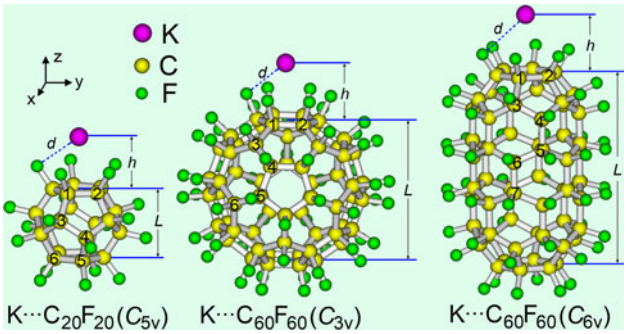

Fig. 1 Optimized geometries at B3LYP/6-31G (d) level

Comparing with the perfluorinated fullerene C_nF_n ($n = 20$ or 60) at the B3LYP/6-31G(d) level, under the effect of the dopant K atom, the semi-cage C_nF_n near the dopant K atom has small distortion while the other semi-cage C_nF_n almost has no distortion. Table 1 shows three small changes for the semi-cage C_nF_n near the dopant K atom. (1) The length of C–C bond in K···C_nF_n is slightly shorter (<0.04 Å) than the corresponding length in C_nF_n ($n = 20$ or 60). (2) The length of C–F bond in the K···C_nF_n is slightly longer (<0.08 Å) than the corresponding length in the C_nF_n ($n = 20$ or 60). (3) From near the K atom to away from the K atom along the z direction, the change degree of the C–C or C–F bond C_nF_n in K···C_nF_n relating to the C_nF_n ($n = 20$ or 60) gradually decreases. As a result,

Table 1 Comparison of the structural parameters (in Å) between K···C_nF_n, and C_nF_n ($n = 20$ or 60) at B3LYP/6-31G(d) level

	K···$C_{20}F_{20}$	$C_{20}F_{20}$	K···$C_{60}F_{60}$	$C_{60}F_{60}$[a]	K···$C_{60}F_{60}$	$C_{60}F_{60}$[a]
Point group	C_{5v}	I_h	C_{3v}	I_h	C_{6v}	D_{6h}
C–C bond						
C1–C2	1.534	1.562 (1.550)	1.577	1.612 (1.607)	1.537	1.569 (1.564)
C1–C3	1.541	1.562 (1.550)	1.604	1.618 (1.613)	1.559	1.576 (1.573)
C3–C4	1.558	1.562 (1.551)	1.608	1.612 (1.607)	1.589	1.593 (1.588)
C4–C5	1.557	1.562 (1.550)	1.617	1.618 (1.613)	1.593	1.595 (1.591)
C5–C6	1.560	1.562 (1.550)	1.610	1.612 (1.613)	1.610	1.612 (1.603)
C6–C7					1.612	1.612 (1.606)
C–F bond						
C1–F1	1.419	1.358 (1.377)	1.434	1.363 (1.368)	1.421	1.362 (1.367)
C3–F3	1.370	1.358 (1.377)	1.370	1.363 (1.368)	1.370	1.360 (1.366)
C4–F4	1.366	1.358 (1.377)	1.366	1.363 (1.368)	1.366	1.362 (1.367)
C5–F5	1.364	1.358 (1.377)	1.364	1.363 (1.368)	1.377	1.375 (1.381)
C6–F6	1.363	1.358 (1.377)	1.363	1.363 (1.368)	1.380	1.379 (1.386)
C7–F7					1.379	1.379 (1.386)
d	2.812		2.770		2.901	
h	2.985		3.045		2.943	
L	3.431	3.486 (3.451)	7.269	7.327 (7.291)	9.959	10.006 (9.978)

[a] See ref 13. The values in parentheses for $e^-@C_nF_n$ ($n = 20$ or 60) at B3LYP/6-31G(d) + dBF level, see ref 22. The lengths of isolated K–F molecule are 2.174 Å at B3LYP/6-31G(d) level and 2.177 Å at CCSD(T)/6-31G(d) level

the diameter (L) is smaller (<0.06 Å) for the K···C_nF_n ($n = 20$ or 60) than for the corresponding C_nF_n.

It is reported that the structure of the $C_{60}F_{60}$ cage in $e^-@C_{60}F_{60}$ relating to the neutral $C_{60}F_{60}$ also has small shortening of C–C bond and elongation of C–F bond under the effect of the excess electron. [52] These change degrees of the C–C or C–F are symmetrical and thus, the symmetry of the molecule has not been decreased. From Table 1, the lengths of C–C bonds near the K atom in K···C_nF_n are even shorter than the corresponding lengths in $e^-@C_nF_n$ ($n = 20$ or 60) while these of C–C bonds away from the K atom in K···C_nF_n are larger than the corresponding lengths in $e^-@C_nF_n$ and close to these in C_nF_n ($n = 20$ or 60). Similarly, the lengths of C–F bonds near the K atom in K···C_nF_n are larger than the corresponding lengths in $e^-@C_nF_n$ ($n = 20$ or 60) while these of C–F bonds away from the K atom in K···C_nF_n are shorter than the corresponding lengths in $e^-@C_nF_n$ and close to these in C_nF_n ($n = 20$ or 60). As a result, the diameter (L) is shorter for the K···C_nF_n than for $e^-@C_nF_n$ ($n = 20$ or 60). Thus, the change degrees of the C–C or C–F in K···C_nF_n relating to the C_nF_n ($n = 20$ or 60) are not symmetrical and thus, the symmetry of the molecule has been decreased.

3.2 Stabilities and infrared spectra

For the K···$C_{20}F_{20}$ (C_{5v}), the dopant K atom is outside a pentagonal ring of the cage to form stable K···$C_{20}F_{20}$ (C_{5v}) as the stable $C_{20}F_{20}$ (I_h) is made of 12 pentagonal rings. When the dopant K atom is outside a pentagonal ring of the $C_{60}F_{60}$ (I_h) cage, the formed K···$C_{60}F_{60}$ (C_{5v}) is a transition state because of an imaginary frequency (59.2i). Therefore, the dopant K atom is outside a hexagonal ring of the $C_{60}F_{60}$ cage to form stable K···$C_{60}F_{60}$ (C_{3v} and C_{6v}) though the corresponding $C_{60}F_{60}$ (I_h and D_{6h}) have both pentagonal and hexagonal rings. By comparing the total energies of K···$C_{60}F_{60}$ (C_{3v} and C_{6v}), Table 2 shows that it is -240.27 kcal/mol lower for K···$C_{60}F_{60}$ (C_{6v}) than for K···$C_{60}F_{60}$ (C_{3v}). Therefore, the former is thermodynamically more stable than the latter.

For the molecular orbital analysis, the energy separation between the highest occupied molecular orbital (HOMO) and the lowest unoccupied molecular orbital (LUMO), *i.e.* HOMO-LUMO gap (E_{gap}), has been used as a simple indicator of kinetic stability. A large E_{gap} implies high kinetic stability and low chemical reactivity [67–70]. It implies that it is unfavorable to be reduced, difficult to add electrons to a high-lying LUMO, difficult to be oxidized, and not easy to extract electrons from a low-lying HOMO. The HOMO-LUMO gap represents the chemical hardness of a molecule [67–70]. Considering the E_{gap} of these K···C_nF_n ($n = 20$ and 60), the E_{gap} value decreases with increasing the diameter of the cage (L) in the order of 2.911 (K···$C_{20}F_{20}$ (C_{5v})) > 1.702 (K···$C_{60}F_{60}$ (C_{3v})) > 1.219 eV (K···$C_{60}F_{60}$ (C_{6v})). A new index proposed by Aihara was a T value, defined as a HOMO-LUMO gap multiplied by the number of conjugated atoms. The T value was applied successfully to fullerenes with up to 100 carbon atoms [71]. We define nE_{gap} as an indicator of kinetic stability (see Table 2). The order of the nE_{gap} is 59.82 (K···$C_{20}F_{20}$ (C_{5v})) < 102.12 (K···$C_{60}F_{60}$ (C_{3v})) > 73.14 (K···$C_{60}F_{60}$ (C_{6v})). This indicates that the size and shape of the perfluorinated fullerene cage influence the kinetic stability of the molecule. That is to say, increasing the cage size (from $C_{20}F_{20}$ to $C_{60}F_{60}$) increases the kinetic stability of the molecule while flattening the shape of the cage (symmetry of original $C_{60}F_{60}$ cage from I_h to D_{6h}) decreases the kinetic stability of the molecule.

At many-electron level, we calculated the ionization potentials (IPs) and electron affinities (EAs) of these K···C_nF_n ($n = 20$ and 60). As shown in Table 2, the order of IPs is 7.066 (K···$C_{20}F_{20}$ (C_{5v})) < 7.422 (K···$C_{60}F_{60}$

Table 2 Total energies (E_{tot}, au); Relative energies E_{rel} (kcal/mol); HOMO-LUMO (E_{gap}, eV); Ionization potentials (IP, eV); Electron affinities (EAs, eV); and Cage deformation energies (E_{def}, kcal/mol) at the B3LYP/6-311 + G(2d) level. Interaction energies (E_{int}, kcal/mol) at M05-2X/6-311 + G(2d) level (B3LYP/6-311 + G(2d) level in parentheses)

	K···$C_{20}F_{20}$ (C_{3v})	K···$C_{60}F_{60}$ (C_{3v})	K···$C_{60}F_{60}$ (C_{6v})	C_{60} (I_h)
E_{tot}	−3358.9254	−8875.4842	−8875.8671	
E_{rel}		0.0	−240.27	
LUMO	−2.623	−4.579	−4.918	
HOMO	−5.614	−6.281	−6.137	
E_{gap}	2.991	1.702	1.219	
IP	7.066	7.422	7.315	7.565
EA	2.888	4.202	3.951	2.554
E_{int}	−78.24 (−64.71)	−93.72 (−78.62)	−88.03 (−71.11)	
E_{def}	10.91	13.21	10.81	

The interaction energy of isolated K–F molecule is −119.37 kcal/mol at M05-2X/6-311 + G(2d)//CCSD(T)/6-31G(d) level or −119.94 kcal/mol at CCSD(T)/6-311 + G(2d)//CCSD(T)/6-31G(d) level

(C_{3v})) > 7.315 eV (K···$C_{60}F_{60}$ (C_{6v})). Comparing the K···$C_{20}F_{20}$ (C_{5v}) with the K···$C_{60}F_{60}$ (C_{3v} or C_{6v}), the IP increases with increasing the perfluorinated fullerene cage size (from $C_{20}F_{20}$ to $C_{60}F_{60}$). Comparing the K···$C_{60}F_{60}$ (C_{3v}) with the K···$C_{60}F_{60}$ (C_{6v}), the IP decreases with decreasing the symmetry of original $C_{60}F_{60}$ cage from I_h to D_{6h}. Therefore, the reducibility of the molecule decreases with increasing the cage size and increases with flattening the shape of the cage. The IP of 7.422 eV for K···$C_{60}F_{60}$ (C_{6v}) is slightly smaller than that of the measured value of 7.61 eV [59, 60] and calculated value of 7.565 eV for the stable C_{60} fullerene, which implies that the reducibility of K···$C_{60}F_{60}$ (C_{6v}) is close to that of the stable C_{60} fullerene.

In Table 2, the order of EAs is 2.888 (K···$C_{20}F_{20}$ (C_{5v})) < 4.202 (K···$C_{60}F_{60}$ (C_{3v})) > 3.951 eV (K···$C_{60}F_{60}$ (C_{6v})). Comparing the K···$C_{20}F_{20}$ (C_{5v}) with the K···$C_{60}F_{60}$ (C_{3v} or C_{6v}), the EA increases with increasing the perfluorinated fullerene cage size (from $C_{20}F_{20}$ to $C_{60}F_{60}$). Comparing the K···$C_{60}F_{60}$ (C_{3v}) with the K···$C_{60}F_{60}$ (C_{6v}), the EA decreases with decreasing the symmetry of original $C_{60}F_{60}$ cage from I_h to D_{6h}. Therefore, the oxidizability of the molecule increases with increasing the cage size and decreases with flattening the shape of the cage. The EAs of 2.888 ~ 4.202 eV for these K···C_nF_n ($n = 20$ and 60) are larger than the calculated value of 2.554 eV for the stable C_{60} fullerene. These results imply that these perfluorinated exohedral compounds are easier to be reduced than the stable C_{60} cage.

The results of IPs and EAs show that the redox properties of these K···C_nF_n ($n = 20$ and 60) may be close to the stable C_{60} fullerene cages, which indicates that they have certain stabilities.

Notice that the interaction energy (E_{int}) between the dopant K atom and perfluorinated fullerene cage C_nF_n can also reflect the stability of the K···C_nF_n ($n = 20$ or 60) molecule. From Table 2, the interaction energies at M05-2X method are about 14 ~ 17 kcal/mol lower than the corresponding results at B3LYP method. According to Truhlar's suggestion, [61, 62] the E_{int} values calculated at the M05-2X method are used in the following discussion. The E_{int} of three K···C_nF_n ($n = 20$ and 60) are large (−78.24 ~ −93.72 kcal/mol) which suggests certain stabilities of these K···C_nF_n ($n = 20$ and 60) molecules. In addition, from Table 2, the C_nF_n in K···C_nF_n ($n = 20$ and 60) have deformation energies (E_{def}) of 10.81 ~ 13.21 kcal/mol due to the small deformations of the cages relating to the corresponding C_nF_n ($n = 20$ and 60). The E_{def} has small effect on the stability of the structure as it contributes a small fraction to the corresponding E_{int}.

To provide more helpful hints to the experimental identifications of the designed perfluorinated exohedral potassium-metallofullerenes, the calculated infrared adsorption spectra are depicted in Fig. 2. There are three obvious vibration modes: pentagon or hexagon (near the K atom) swaying mode, cage stretching mode (in the z axis direction), and cage distorting mode. From Fig. 2, three characteristics for the vibrational frequencies and

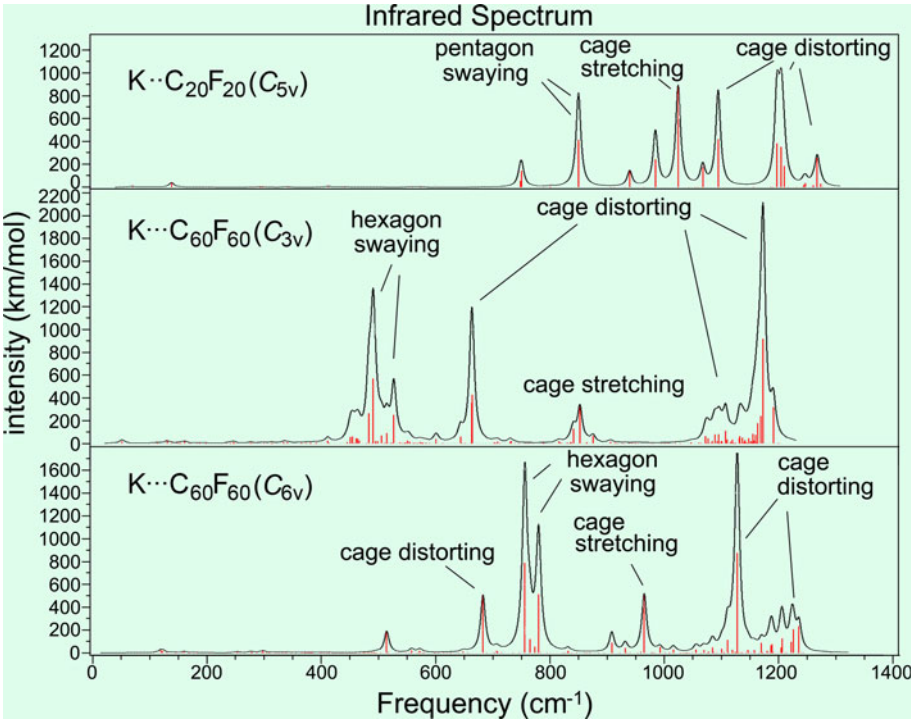

Fig. 2 Calculated infrared adsorption spectra for the three structures

adsorption intensities are shown. (1) The redshift from K···$C_{20}F_{20}$ (C_{5v}) to K···$C_{60}F_{60}$ (C_{3v}) and blueshift from K···$C_{60}F_{60}$ (C_{3v}) to K···$C_{60}F_{60}$ (C_{6v}) are observed for the peaks corresponding to both pentagon or hexagon swaying mode and cage stretching mode. (2) The IR intensity of the peak corresponding to cage stretching mode decreases from K···$C_{20}F_{20}$ (C_{5v}) to K···$C_{60}F_{60}$ (C_{3v} or C_{6v}). (3) The redshift of a peak corresponding to cage distorting mode is observed from K···$C_{20}F_{20}$ (C_{5v}) to K···$C_{60}F_{60}$ (C_{3v} or C_{6v}).

3.3 $K^+\cdots C_nF_n^-$ ($n = 20$ or 60) ionic bond

In these K···C_nF_n ($n = 20$ or 60), the C_nF_n cage ($n = 20$ or 60) has 20 or 60 exo polar C–F bonds. From analysis of natural bond orbital (NBO) charge (see Fig. 3), the polarized C–F bonds constitute an approximate $C^{\delta+}$–$F^{\delta-}$ double electric layer due to the negatively charged outer F shell and the positively charged inner C shell. Owing to such double electric layer in each cage of these K···C_nF_n ($n = 20$ or 60) structures, an interior electronic attractive potential [51–53] is formed. This attractive potential provides a possibility to encapsulate an excess electron inside the cage.

The NBO charges of the three K atoms in these K···C_nF_n ($n = 20$ or 60) are positive, and the range of them is $0.842 \sim 0.916$. These results show the valence K atom is +1. Likewise, the $-0.842 \sim -0.916$ for the range the NBO charges of C_nF_n ($n = 20$ and 60) cages indicate valence of C_nF_n cage in each structure is -1. In this case, the K atom loses an electron, and C_nF_n cage obtains an electron to form K^+ cation and $C_nF_n^-$ anion. To confirm it, the singly occupied molecular orbitals (SOMO) of the three structures are depicted in Fig. 4a, in which the electron cloud is mainly located at the $C_{60}F_{60}$ cage. Thus, these perfluorinated exohedral compounds can be denoted as $K^+\cdots C_nF_n^-$ ($n = 20$ or 60). An electron has transferred from K atom to the perfluorinated cage ($C_{20}F_{20}$ or $C_{60}F_{60}$) to form excess electron and $K^+\cdots C_nF_n^-$ ($n = 20$ or 60) ionic bond. It is reported that the planar structure has unusual spatial charge-spin separation for neutral and anionic gold defamers [72]. Figure 3 indicates both the NBO charge and the spin density are different in different regions, and both of them gradually decrease from near to away from the K atom along the z direction. Therefore, these K···C_nF_n ($n = 20$ or 60) are charge-spin separation.

Kim and co-workers found the peculiar change in magnetic property (from diamagnetic to paramagnetic) of the dianionic C60-dimer [73]. For the K···C_nF_n ($n = 20$ or 60), under the doping effect of K atom, the singlet C_nF_n changes into doublet $C_nF_n^-$ ($n = 20$ or 60). Therefore, a change in magnetic property should be also shown from C_nF_n to $C_nF_n^-$ ($n = 20$ or 60).

The interaction energies are $-78.24 \sim -93.72$ kcal/mol. At the same level, these energies are smaller than the

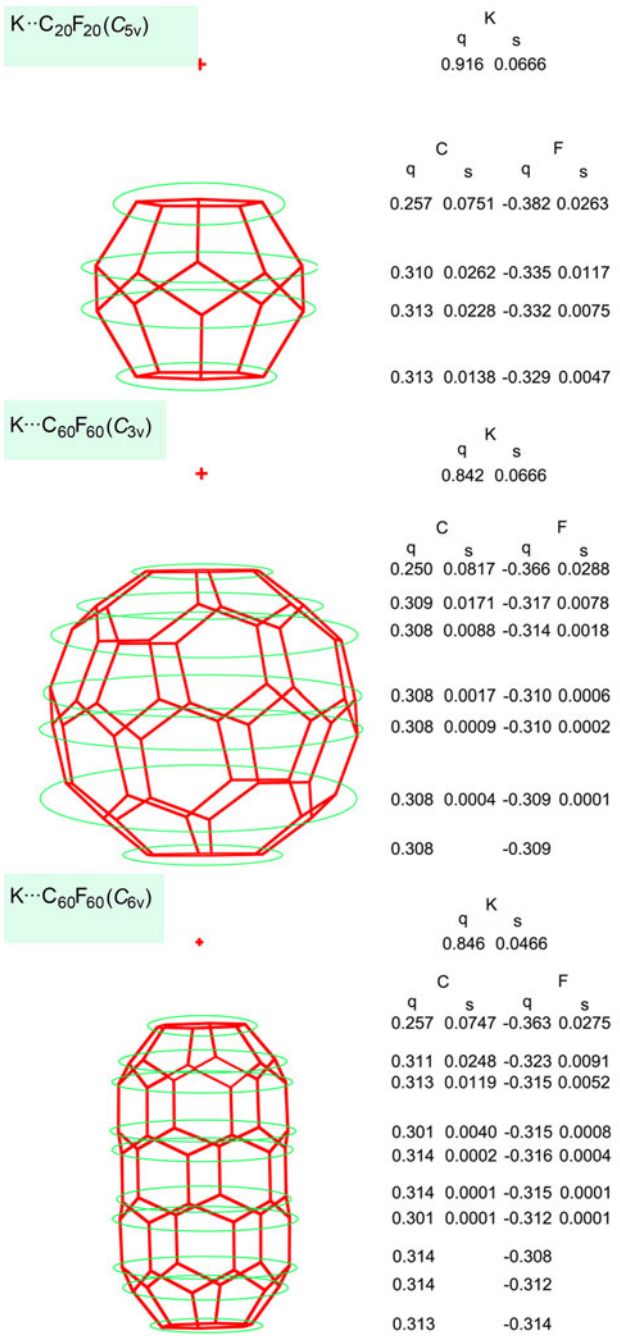

Fig. 3 Natural bond orbital (q) charges and spin density (s) at B3LYP/6-31G (d) level

interaction energy between K^+ and F^- in the isolated KF molecule (−119.37 kcal/mol) as the distances between the K^+ and $C_nF_n^-$ ($h > 2.9$ Å) are smaller than that between K^+ and F^- in the isolated KF molecule (2.174 Å).

3.4 Partial interior and surface excess electron state

Since the electron is distributed to the cage to form excess electron, it is wondering how about the effect of the

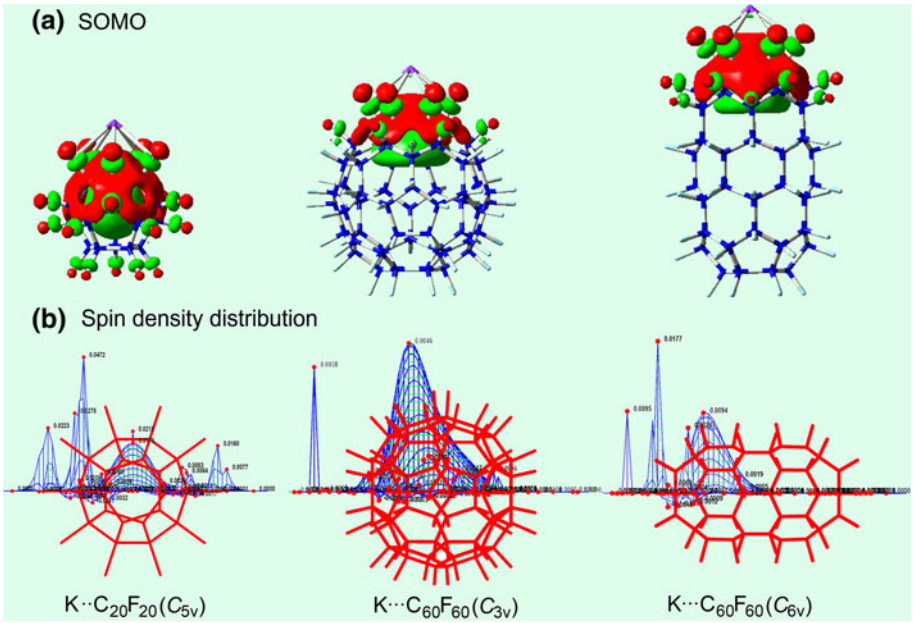

Fig. 4 **a** SOMO at isovalue of 0.025 au, and **b** spin density maps at the isovalue of 0.0002 au for the three structures

counterion metal cation (K^+) on the location of the excess electron? In order to identify the location of the excess electron, the SOMOs of these $K^+\cdots C_nF_n^-$ ($n = 20$ or 60) are presented in Fig. 4a.

As given in Fig. 4a, the green sphere or hemisphere in SOMO of $K^+\cdots C_nF_n^-$ ($n = 20$ or 60) shows that the partial electron cloud is located within the C_nF_n ($n = 20$ or 60) cage, while the red bowl indicates that the other partial electron cloud is mainly dispersed on the surface of the C_nF_n ($n = 20$ or 60) cage. Those imply the excess electron is partially located in the interior and partially dispersed on the surface of the C_nF_n ($n = 20$ or 60) cage.

For further confirmation of the excess electron location, the spin density of $K^+\cdots C_nF_n^-$ ($n = 20$ or 60) was evaluated and presented in Fig. 4b. The blue contour is the excess electron spin density distribution. From Fig. 4b, the excess electron spin density distribution indicates that the partial spin density in $K^+\cdots C_nF_n^-$ ($n = 20$ or 60) is located in the interior, and the other partial is dispersed on the surface of the C_nF_n ($n = 20$ or 60) cage. These spin density results are well in accordance with the electron cloud results in the SOMOs.

Therefore, it can be concluded that the excess electron is partially located in the interior and partially dispersed on the surface of the C_nF_n ($n = 20$ or 60) cage to form excess electron with partial interior and partial surface state.

For the single molecular solvated electron $e^-@C_nF_n$ ($n = 20$ or 60), [51, 52] it is reported that the excess electron is mainly located in the interior of the $C_{60}F_{60}$ cage. So, why the excess electron is partially located in the interior and partially dispersed on the surface of the C_nF_n cage in the $K\cdots C_nF_n$ ($n = 20$ or 60)? To further understand the evolution of the location of excess electron, we

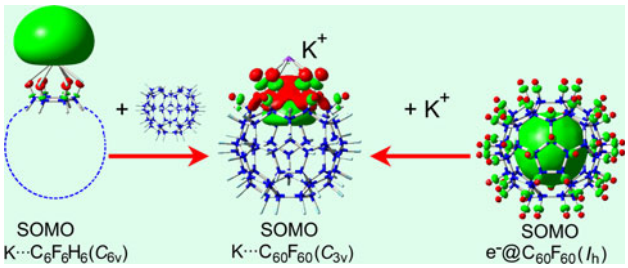

Fig. 5 Effects of the cage and the counterion on the location of the excess electron

comparing the SOMO of a bowl-shaped $K\cdots C_6F_6H_6$ (C_{6v}) mode with these of $K\cdots C_{60}F_{60}$ (C_{3v}) and $e^-@C_{60}F_{60}$. The $K\cdots C_6F_6H_6$ (C_{6v}) model is taken from equilibrium geometry of the $K\cdots C_{60}F_{60}$ (C_{3v}) by fixing the geometries of K atom and the two neighboring hexagonal rings (F_6 and C_6) in the $K\cdots C_{60}F_{60}$ (C_{3v}), removing the rest, and adding six H atom to satisfy the sp^3 bonding states of carbon atom.

From Fig. 5, the electron cloud in the SOMO of $K\cdots C_6F_6H_6$ is pushed out by the bowl ($C_6F_6H_6$) to form diffusive excess electron cloud (large green sphere). Adding an open perfluorinated cage into $K\cdots C_6F_6H_6$ to form $K\cdots C_{60}F_{60}$ (C_{3v}), the excess electron cloud (large green sphere) is pulled from outside of $C_6F_6H_6$ to the interior and the surface of perfluorinated cage $C_{60}F_{60}$. Therefore, the perfluorinated cage $C_{60}F_{60}$ has obvious electron-pull effect. The electron cloud in the SOMO of the solvated electron $e^-@C_{60}F_{60}$ (I_h) is mainly located inside the perfluorinated cage $C_{60}F_{60}$ (large green sphere), adding a counterion cation K^+ upper the $e^-@C_{60}F_{60}$ (I_h) to form $K^+\cdots C_{60}F_{60}^-$, and it can be found that partial excess electron is pulled

from the interior to the surface of the cage $C_{60}F_{60}$. Thus, the counterion cation also has obvious electron-pull effect.

Comparing with the single solvated electron systems $e^-@C_nF_n$ ($n = 20$ and 60), these $K^+\cdots C_nF_n^-$ ($n = 20$ and 60) compounds have much larger IPs. The IPs of $K^+\cdots C_nF_n^-$ ($n = 20$ and 60) are 7.066 $\sim$ 7.422 eV, while the IPs of $e^-@C_{20}F_{20}$ (I_h), $e^-@C_{60}F_{60}$ (I_h), and $e^-@C_{20}F_{20}$ (D_{6h}) are 3.66 (or 3.40) [50, 51], 4.95 [52], and 4.67 eV [52], respectively. These results show that the IP of the molecule considerably increases under the effect of counterion K^+. Thererfore, the existence of the counterion remarkably increases the stability of the molecule.

3.5 Polarizabilities and electronic absorption spectra

The important electric properties should be considered for these perfluorinated exohedral compounds. Owing to the interpolarization between K and C_nF_n cage, these $K\cdots C_nF_n$ ($n = 20$ or 60) exhibit large dipole moment in z direction (μ_z). From Table 3, the order of the resulting molecular dipole moments (μ_0) of them is 5.6165 ($K\cdots C_{20}F_{20}$ (C_{5v})) < 7.5614 ($K\cdots C_{60}F_{60}$ (C_{3v})) > 7.1052 au ($K\cdots C_{60}F_{60}$ (C_{6v})). Comparing the $K\cdots C_{20}F_{20}$ (C_{5v}) with the $K\cdots C_{60}F_{60}$ (C_{3v} or C_{6v}), the μ_0 increases with increasing the perfluorinated fullerene cage size (from $C_{20}F_{20}$ to $C_{60}F_{60}$). Comparing the $K\cdots C_{60}F_{60}$ (C_{3v}) with the $K\cdots C_{60}F_{60}$ (C_{6v}), the μ_0 decreases with decreasing the symmetry of original $C_{60}F_{60}$ cage (from I_h to D_{6h}). From Table 3, the order of the static polarizabilities (α_0) is 222.99 ($K\cdots C_{20}F_{20}$ (C_{5v})) < 679.70 ($K\cdots C_{60}F_{60}$ (C_{3v})) > 631.58 au ($K\cdots C_{60}F_{60}$ (C_{6v})), which indicates that the α_0 increases with increasing the perfluorinated fullerene cage size and decreases with decreasing the symmetry of original $C_{60}F_{60}$ cage. Therefore, both the dipole moment and the static polarizability of the perfluorinated exohedral compound increase with increasing the cage size and decrease with flattening the shape of the cage. In addition, the order of the anisotropy of the polarizabilities ($\Delta\alpha$) is 19.73 ($K\cdots C_{20}F_{20}$ (C_{5v})) < 52.19 ($K\cdots C_{60}F_{60}$ (C_{3v})) < 631.58 au ($K\cdots C_{60}F_{60}$ (C_{6v})).

Table 3 Dipole moment (μ_0, au); Polarizability (α_0, au); and Anisotropy of the polarizability ($\Delta\alpha$, au) at HF/6-31 + g(d) level

	$K\cdots C_{20}F_{20}$ (C_{5v})	$K\cdots C_{60}F_{60}$ (C_{3v})	$K\cdots C_{60}F_{60}$ (C_{6v})
μ_x	0.0000	0.0000	0.0000
μ_y	−0.0007	−0.0002	0.0000
μ_z	5.6165	7.5614	7.1052
μ_0	5.6165	7.5614	7.1052
α_x	216.41	662.30	563.35
α_y	216.41	662.30	563.36
α_z	236.15	714.49	768.02
α_0	222.99	679.70	631.58
$\Delta\alpha$	19.73	52.19	204.67

For these $K\cdots C_nF_n$ ($n = 20$ or 60), the excess electron absorption spectra at CIS/6-31G(d) level are presented in Fig. 6a. From Fig. 6a, there are two low-lying crucial transition absorption peaks with large oscillator strengths (> 0.10) for each of these molecules. The diagram of these two electronic excitations and the contour plots for their corresponding molecular orbitals are presented in Fig. 6b. From Fig. 6b, the first electron transition is localized in one cage, and the electronic excitation corresponds to two degenerate $s \rightarrow p$ transitions (from HOMO to LUMO + 5 and LUMO + 6 for $K\cdots C_{20}F_{20}$ (C_{5v}) and from HOMO to LUMO + 2 and LUMO + 3 for $K\cdots C_{60}F_{60}$ (C_{3v} and C_{6v})). The transition energies are 2.620 ($K\cdots C_{20}F_{20}$ (C_{5v})), 1.616 ($K\cdots C_{60}F_{60}$ (C_{3v})), and 1.977 eV ($K\cdots C_{60}F_{60}$ (C_{6v})). These transition energies are comparable with some excess electron systems. For example, the first transition energies of the (HCN)···Li [36], and Na_nF_{n-1} ($n \leq 6$) [74] are lying in the range of 0.95 $\sim$ 1.5 eV. For the hydrated electron cluster $(H_2O)_n^-$ ($n \rightarrow \infty$), the first transition energy is 1.977 or 1.947 eV [53, 75]. The second electron transition (third of $K\cdots C_{60}F_{60}$ (C_{3v})) is from inside of the perfluorinated cage to above the K atom, and the electronic excitation corresponds to $s \rightarrow s$ transitions (from HOMO to LUMO). The transition energies are 2.661 ($K\cdots C_{20}F_{20}$ (C_{5v})), 2.933 ($K\cdots C_{60}F_{60}$ (C_{3v})), and 2.929 eV ($K\cdots C_{60}F_{60}$ (C_{6v})).

Comparison of these spectra reveals two obvious characteristics for these two crucial absorption peaks. (1) From $K\cdots C_{20}F_{20}$ (C_{5v}) to $K\cdots C_{60}F_{60}$ (C_{3v}) and to $K\cdots C_{60}F_{60}$ (C_{6v}), red-shift from 473.27 to 767.21 nm and then blue-shift to 627.27 nm for the first absorption peak while blue-shift from 465.96 to 422.67 and then 423.26 nm for the second absorption peak are observed. (2) Both the changes of oscillator strengths for the two absorption peaks decrease from $K\cdots C_{20}F_{20}$ (C_{5v}) to $K\cdots C_{60}F_{60}$ (C_{3v}) and then increase from $K\cdots C_{60}F_{60}$ (C_{3v}) to $K\cdots C_{60}F_{60}$ (C_{6v}). These provides a possibility of influencing the excess electron absorption by changing the molecular structures (cage size and shape), which may be important for the design of the new optical and photoelectric materials or devices with good performances.

4 Conclusions

In this work, we have reported the structures and properties of three perfluorinated exohedral metallofullerenes, $K\cdots C_{20}F_{20}$ (C_{5v}), $K\cdots C_{60}F_{60}$ (C_{3v}), and $K\cdots C_{60}F_{60}$ (C_{6v}) for the first time.

In these exohedral compounds, it is found that an electron transfers from K atom to the perfluorinated cage ($C_{20}F_{20}$ or $C_{60}F_{60}$) to form excess electron and long

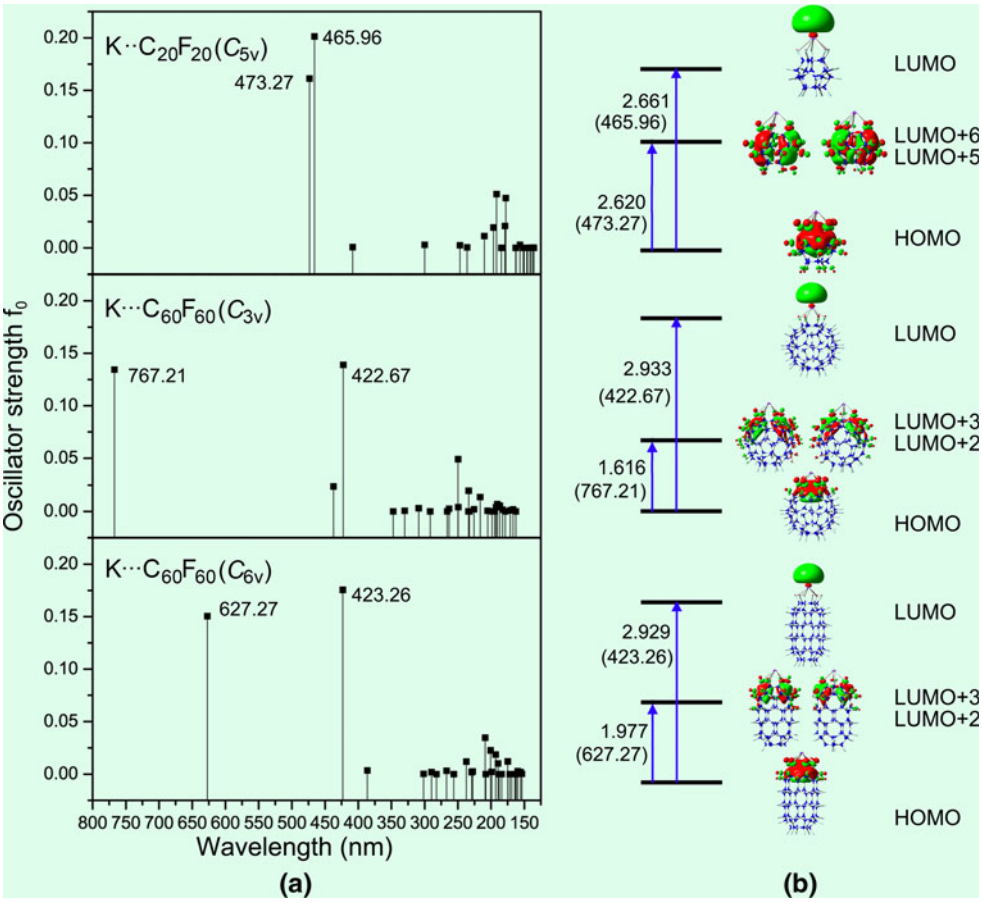

Fig. 6 **a** Excess electronic absorption spectra for the three structures, and **b** energy diagram for two main excited states (excitation energies in eV) at CIS/6-31G (d) level for the three structures. The value in parentheses corresponds to the wavelength value (in nm)

$K^+\cdots C_nF_n^-$ ($n = 20$ or 60) ionic bond (length > 2.9 Å). The resulting interaction energies are -78.24 ~ -93.72 kcal/mol.

Comparing to the solvated electron $e^-@C_nF_n$ ($n = 20$ or 60) with interior state, [51, 52] under the effect of counterion K^+, partial excess electron is pulled from the interior to the surface of the cage and form excess electron with partial interior and surface state.

Comparing to ionization potentials (3.40 ~ 4.95 eV [50–52]) of the solvated electron $e^-@C_nF_n$ ($n = 20$ or 60), these $K^+\cdots C_nF_n^-$ ($n = 20$ or 60) have much larger ionization potentials of 7.066 ~ 7.422 eV, which indicates the larger stabilities of them. Those suggest that the existence of the counterion remarkably increases the stability of the molecule.

The cage size and shape effects on the dipole moment, polarizability, and excess electron transitions are exhibited, which may be important for the design of the new optical and photoelectric materials or devices with good performances.

Acknowledgments This work was supported by the National Natural Science Foundation of China (No. 20773046).

References

1. Kroto HW, Heath JR, O'Brien SC, Curl RF, Smalley RE (1985) Nature 318:162 (London)
2. Krátschmer W, Lamb LD, Fostiropoulos K, Huffman DR (1990) Nature 347:354 (London)
3. Bethune DS, Johnson RD, Salem JR, De Vries MS, Yannoni CS (1993) Nature 366:123 (London)
4. Shinohara H (2000) Rep Prog Phys 63:843
5. Shinohara H, Tanaka M, Sakata M, Hashizume T, Sakurai T (1996) Mater Sci Forum 232:207
6. Vostrowsky O, Hirsch A (2006) Chem Rev 106:5191
7. Park JM, Tarakeshwar P, Kim KS (2000) J Chem Phys 116:10684
8. Loboda O, Jensen VR, Borve KJ (2006) Fullerenes Nanotubes Carbon Nanostruct 14:365
9. Lu G, Deng K, Wu H (2006) J Chem Phys 124(5):54305
10. Hutchison K, Gao J, Schick G, Rubin Y, Wudl F (1999) J Am Chem Soc 121:5611
11. Makarova TL, Sundqvist B, HNhne R, Esquinazi P, Kopelevich Y, Scharff P, Davydov VA, Kashevarova LS, Rakhmanina AV (2001) Nature 413:716
12. Bendikov M, Wudl F, Perepichka DF (2004) Chem Rev 104:4891
13. Nishibayashi Y, Saito M, Uemura S, Takekuma S-I, Takekuma H, Yoshida Z-i (2004) Nature 428:279
14. Nakamura E, Isobe H (2003) Acc Chem Res 36:807
15. Stephens A, Green MLH (1997) Adv Inorg Chem 44:1
16. Mathur P, Mavunkal IJ, Umbarkar SB (1998) J Cluster Sci 9:393
17. Balch AL, Olmstead MM (1998) Chem Rev 98:2123

18. Govindaraj A, Satishkumar BC, Nath M, Rao CNR (2000) Chem Mater 12:202
19. Hermans S, Sloan J, Shephard DS, Johnson BFG, Green MLH (2002) Chem Commun 276
20. Prinzbach H, Weber K (1994) Angew Chem Int Ed Engl 33:2239
21. Wahl F, Weiler A, Landenberger P, Sackers E, Voss T, Haas A, Lieb M, Hunkler D, Wörth J, Knothe L, Prinzbach H (2006) Chem Eur J 12:6255
22. Cioslowski J, Edgington L, Stefanov BB (1995) J Am Chem Soc 117:10381
23. Holloway JH, Hope EG, Taylor R, Langley JG, Avent AG, Dennis TJ, Hare JP, Kroto HW, Walton DRM (1991) J Chem Soc Chem Commun 966
24. Scuseria GE (1991) Chem Phys Lett 176:423
25. Scuseria GE, Odom GK (1992) Chem Phys Lett 195:531
26. Kudin KN, Bettinger HF, Scuseria GE (2001) Phys Rev B 63:045413
27. Bettinger HF, Kudin KN, Scuseria GE (2001) J Am Chem Soc 123:12849
28. Jia J, Wu H-S, Xu X-H, Zhang X-M, Jiao H (2008) J Am Chem Soc 130:3985
29. Hart EJ, Boag JW (1962) J Am Chem Soc 84:4090
30. Hammer NI, Shin J-W, Headrick J, Diken EG, Roscioli JR, Weddle GH, Johnson MA (2004) Science 306:675
31. Verlet JR, Bragg AE, Kammrath A, Cheshnovsky O, Neumark DM (2005) Science 307:93
32. Page CC, Moster CC, Chen X, Dutton L (1999) Nature 402:47 (London)
33. Tributsch H, Pohlmann L (1998) Science 279:1891
34. Desfrançois C, Carles S, Schermann JP (2000) Chem Rev 100:3943
35. Lee HM, Lee S, Kim KS (2003) J Chem Phys 119:187
36. Li Y, Li Z-R, Wu D, Li RY, Hao XY, Sun C-C (2004) J Phys Chem B 108:3145
37. Chen W, Li Z-R, Wu D, Li R-Y, Sun C-C (2005) J Phys Chem B 109:601
38. Matsuishi S, Toda Y, Miyakawa M, Hayashi K, Kamiya T, Hirano M, Tanaka I, Hosono H (2003) Science 301:626
39. Chiesa M, Paganini MC, Giamello E, Murphy DM, Di Valentin C, Gb Pacchioni (2006) Acc Chem Res 39:861
40. Edwards PP, Anderson PA, Thomas JM (1996) Acc Chem Res 29:23
41. Srdanov VI, Stucky GD, Lippmaa E, Engelhardt G (1998) Phys Rev Lett 80:2449
42. Bragg AE, Verlet JRR, Kammrath A, Cheshnovsky O, Neumark DM (2004) Science 306:669
43. Turi L, Sheu W-S, Rossky PJ (2005) Science 309:914
44. Coe JV, Lee GH, Eaton JG, Arnold ST, Sarkas HW, Bowen KH, Ludewigt C, Worsnop DR (1990) J Chem Phys 92:3980
45. Barnett RN, Landman U, Scharf D, Jortner J (1989) Acc Chem Res 22:350
46. Coe JV (2001) Int Rev Phys Chem 20:33
47. Jordan KD (2004) Science 306:618
48. Sommerfeld T, Jordan KD (2006) J Am Chem Soc 128:5828
49. Paul A, Wannere CS, Kasalova V, Schleyer Paul VR, Schaefer HF III (2005) J Am Chem Soc 127:15457
50. Irikura KK (2008) J Phys Chem A 112:983
51. Zhang C-Y, Wu H-S, Jiao H (2007) J Mol Model 13:499
52. Wang Y-F, Li Z-R, Wu D, Sun C-C, Gu FL (2010) J Comput Chem 31:195
53. Simons J (2008) J Phys Chem A 112:6401
54. Reed AE, Weinstock RB, Weinhold F (1985) J Chem Phys 83:735
55. Carpenter JE, Weinhold F (1988) J Mol Struct 169:41 (THEOCHEM)
56. Rienstra-Kiracofe JC, Tschumper GS, Schaefer HF III, Sreela N, Ellison GB (2002) Chem Rev 102:231
57. Shkrob IA (2007) J Phys Chem A 111:5223
58. Zimmerman JA, Eyler JR, Bach SBH, McElvany SW (1991) J Chem Phys 94:3556
59. Paul A, Wannere CS, Kasalova V, Schleyer Paul VR, Schaefer HF III (2005) J Am Chem Soc 127:15457
60. Khan A (2005) Chem Phys Lett 401:85
61. Zhao Y, Schultz NE, Truhlar DG (2006) J Chem Theory Comput 2:364
62. Zhao Y, Truhlar DG (2008) Theor Chem Acc 120:215
63. Szalewicz K, Jeziorski B (1999) J Chem Phys 109:1198
64. Boys SF, Bernardi F (1970) Mol Phys 19:553
65. Hobza P, Havlas Z (1998) Theor Chem Acc 99:372
66. Frisch MJ, Trucks GW, Schlegel HB, Scuseria GE, Robb MA, Cheeseman JR, Montgomery JA Jr, Vreven T, Kudin KN, Burant JC, Millam JM, Iyengar SS, Tomasi J, Barone V, Mennucci B, Cossi M, Scalmani G, Rega N, Petersson GA, Nakatsuji H, EharaM HadaM, Toyota K, Fukuda R, Hasegawa J, Shida M, Nakajima T, Honda Y, Kitao O, Nakai H, Klene M, Li KnoxJE, Hratchian HP, Cross JB, Bakken V, Adamo C, Jaramillo J, Gomperts R, Stratmann RE, Yazyev O, Austin AJ, Cammi R, Pomelli C, Ochterski JW, Ayala PY, Morokuma K, Voth GA, Salvador P, Dannenberg JJ, Zakrzewski VG, Dapprich S, Daniels AD, Strain MC, Farkas O, Malick DK, Rabuck AD, Raghavachari K, Foresman JB, Ortiz JV, Cui Q, Baboul AG, Clifford S, Cioslowski J, Stefanov BB, Liu G, Liashenko A, Piskorz P, Komaromi I, Martin RL, Fox DJ, Keith T, Al-Laham MA, Peng CY, Nanayakkara A, Challacombe M, Gill PMW, Johnson B, Chen W, Wong MW, Gonzalez C, Pople JA (2004) Gaussian 03, revision E.01. Gaussian Inc., Wallingford, CT
67. Zhou Z, Parr RG, Garst JF (1988) Tetrahedron Lett 29:4843
68. Zhou Z, Parr RG, Garst JF (1989) J Am Chem Soc 111:7371
69. Zhou Z, Parr RG (1990) J Am Chem Soc 112:5720
70. Parr RG, Zhou Z (1993) Acc Chem Res 26:256
71. Aihara J (1999) J Phys Chem A 103:7478
72. Choi YC, Kim WY, Lee HM, Kim KS (2009) J Chem Theory Comput 5:1216
73. Kim KS, Park JM, Kim J, Suh SB, TarakeshwarP, Lee HM, Park SS (2000) 11: 2425
74. Durand G, Spiegelmann F, Poncharal PH, Labastie P, ĽHermite J-M, Sence M (1999) J Chem Phys 110:7884
75. Coe JV, Williams SM, Bowen KH (2008) Int Rev Phys Chem 27:27